To appear in *Stochastic Models* (1998)

# Point Process Models for Self-Similar[1] Network Traffic, with Applications

**Bo Ryu**
Networking and Information Exploitation Department
Hughes Research Laboratories
3011 Malibu Canyon Rd., Malibu, CA 90265, USA

**Steven B. Lowen**
Department of Electrical and Computer Engineering
College of Engineering, Boston University
44 Cummington Street, Boston, MA 02215, USA

**Abstract** Self-similar processes based on fractal point processes (FPPs) provide natural and attractive network traffic models. We show that the point process formulation yields a wide range of FPPs which in turn yield a diversity of parsimonious, computationally efficient, and highly practical asymptotic second-order self-similar processes. Using this framework, we show that the relevant second-order fractal characteristics such as long-range dependence (LRD), slowly-decaying variance, and $1/f$ noise are completely characterized by three fundamental quantities: mean arrival rate, Hurst parameter, and fractal onset time. Four models are proposed, and the relationship between their model parameters and the three fundamental quantities are analyzed. By successfully applying the proposed models to Bellcore's Ethernet traces, we show that the FPP models prove useful in evaluating and predicting the queueing performance of various types of fractal traffic sources.

**Keywords**: point process, fractal, self-similarity, long-range dependence, traffic modeling

[1]Throughout this paper, *self-similarity* refers to *asymptotic second-order self-similarity* [4], [13] unless otherwise defined.

# 1 INTRODUCTION

Recent analyses of high-quality traffic measurements have revealed the prevalence of self-similarity (fractal behavior) in local area network (LAN) [13], wide area network (WAN) [30], and compressed video traffic [2], [10]. Self-similarity, a concept coined by Mandelbrot [24], was first explored in the context of computer network traffic by Leland, Taqqu, Willinger, and Wilson [13], who applied it to Ethernet traffic at the Bellcore Research Center [9]. The existence of self-similarity in teletraffic behavior has led to new perspectives and raised questions regarding the evaluation of network performance (see e.g. [7], [12], [35]).

Various stochastic models and techniques have been proposed for modeling the distinctive statistical nature of self-similar network traffic and its effects on network performance. These include Chaotic Maps [8], [31], Cox's $M/G/1$ type models [4], [14], [28], fractional Gaussian noise [10], [28], fractional Brownian motion [25], [26], and Markovian models [32].

In this work, we show that Fractal Point Processes (FPPs) provide novel tools for understanding, modeling and analyzing diverse types of self-similar traffic behavior [35], [36], [37], [42]. In contrast to other approaches, the point process formulation concerns the *dynamics of individual arrivals* and how this gives rise to self-similarity of packet counts in a mathematically rigorous manner. This formulation yields models exhibiting LRD, $1/f$ noise, and slowly-decaying variance, and broadens the range of stochastic processes manifesting self-similarity beyond that achieved by On/Off processes [14], [40], [43] and Gaussian processes [26].

We present four fractal point processes: the fractal renewal process (FRP), the superposition of several fractal renewal processes (Sup-FRP), the fractal-shot-noise-driven Poisson process (FSNDP), and the fractal-binomial-noise-driven Poisson process (FBNDP). These processes were first proposed and analyzed by Lowen and Teich in connection with a series of papers for modeling various statistical phenomena arising in physics and biology [15], [16], [20], [21], [22]. In this work, we show how these processes may be extended to self-similar network traffic. Fractal point processes produce asymptotically second-order self-similar processes (and therefore exhibit LRD), and thus these processes prove highly suitable for modeling various types of self-similar packet traces, much as they do for physical and biological phenomena. For the purposes of simulation, the original models have been tailored to make them compactly parameterized, computationally efficient, and accurate [37].

We begin by investigating the second-order statistical properties of fractal point processes, and show that three parameters suffice to completely quantify the three relevant second-order fractal properties (LRD, 1/f noise, slowly-decaying variance): the mean arrival rate, the fractal exponent (or Hurst parameter), and the fractal onset time. We call these the *three fundamental quantities* and denote them by ($\lambda$, $H$, $T_0$), respectively. We provide a proof of the self-similar nature of these processes, a key contribution which satisfies a requirement for FPPs to apply to network traffic. Next, we provide two methods which yield parsimonious, flexible, and easy-to-generate fractal point processes: one based on renewal processes, and the other on doubly stochastic Poisson processes (DSPPs). The FRP and Sup-FRP belong to the former, while the FSNDP and FBNDP belong to the latter. The DSPP method yields a rich set of Fractal Modulated Poisson Processes just as Markov Modulated Poisson Processes are constructed.

We investigate the relations between the parameters of each of the four models and ($\lambda$, $H$, $T_0$). Lastly, we analyze two Bellcore packet traces, with differing bursty behavior, and characterize both of them with appropriate FPP models. Queueing simulation results show that the buffer overflow probabilities of the matched models are in good agreement with those of the original traces over a wide range of buffer sizes.

# 2 FRACTAL POINT PROCESSES

## 2.1 Introduction

Broadly speaking, fractals are objects which possess a form of self-similarity; parts of the whole can be made to fit to the whole in some way by scaling [16], [24]. Thus scaling and fractals are closely related.

The close relation between scaling and fractals in geometry also holds in one-dimensional stochastic processes. One definition of a fractal stochastic process is one in which the sample paths of the stochastic process have non-integer dimensions; the expected measure of the sample path included within some radius scales with the size of the radius [24]. Since this is but one statistic of the process, we call a stochastic process fractal if several of the relevant statistics exhibit scaling [19], [20], [21], [22], [41].

Likewise, we may call a stochastic *point* process fractal when a number of the relevant statistics exhibit scaling with related scaling exponents, indicating that the represented phenomenon contains clusters of points over all (or a relatively large set of) time or length scales [24], [42]. Since scaling leads mathematically to power-law relations in the scaled quantities [22], a fractal process often has its statistics mathematically expressed by power-law functions. We note that for a general point process, fractal scaling in one statistic does not necessarily imply fractal scaling in other statistics; if scaling exists in only one statistic, then we do not call this process fractal [16], [22].

It is natural to view network traffic as a realization of a stochastic point process; each packet (or cell) arrival is associated with an arrival epoch. Therefore, we call a network traffic trace fractal when several estimated statistics exhibit power-law behavior over a wide range of time and frequency scales. As mentioned earlier, many recent high-quality measurement studies on LAN, WAN, and variable-bit-rate video traffic in a variety of contexts prove to be fractal [2], [10], [13], [30], [34], [38]. We employ only stationary FPP models in this paper, although fractal behavior may be observed from traces which appear to be non-stationary [6].

## 2.2 Second-order statistical measures

Important second-order statistics for an FPP include the power spectral density (PSD), coincidence rate (CR), index of dispersion for counts (IDC) [also called the Fano factor], and count-based covariance function (COV).

The CR measures the correlation between pairs of arrivals (events) with a specified time

delay between them, regardless of intervening arrivals, and is related to the autocorrelation function used with continuous processes [5]. It is defined as

$$G(\tau) \equiv \lim_{\Delta \to 0} \frac{\Pr\{\mathcal{E}(0,\Delta) \text{ and } \mathcal{E}(\tau, \tau+\Delta)\}}{\Delta^2}, \tag{1}$$

where $\mathcal{E}(s,t)$ denotes the occurrence of at least one event of the point process in the half-open interval $[s,t)$. A closely related formulation of (1) involves the autocorrelation of a point process $dN(t)$ [1]:

$$G(\tau) = \mathrm{E}\left[\frac{dN(t)}{dt}\frac{dN(t+\tau)}{dt}\right], \tag{2}$$

where the counting process $N(t)$ refers to the number of events between the time origin and a time $t$. We will use (2) instead of (1) since it proves more convenient. For the PSD, we employ $P(\omega)$ derived directly from the point process itself, and equal to the Fourier transfer of the CR. Another useful statistic is the IDC $F(T)$ which is defined as the variance of the number of arrivals in a specified time window of width $T$ divided by the mean number of arrivals, i.e.,

$$F(T) \equiv \mathrm{Var}[N(T)]/\mathrm{E}[N(T)].$$

Finally, the COV $C(k;T)$ is defined as the covariance between the number of arrivals in two counting windows of counting time $T$ and separation $kT$. If we define $X_k$ as the number of packets (cells) that have arrived during the $k$-th time interval of size $T$ sec, i.e.,

$$X_k \equiv N[kT] - N[(k-1)T],$$

then

$$C(k;T) \equiv \mathrm{Cov}(X_n, X_{n+k}). \tag{3}$$

These four second-order statistics (IDC, PSD, COV, CR) may be obtained from each other by means of the following invertible relations [22], [33]

$$\begin{aligned} F(T) &= (\lambda T)^{-1}\int_{-T}^{T}(T-|\tau|)\left[G(\tau)-\lambda^2\right]d\tau \\ P(\omega) &= \int_{-\infty}^{\infty} G(\tau)e^{-j\omega\tau}\,d\tau \\ C(k;T) &= \int_{-T}^{T}(T-|\tau|)\left[G(kT+\tau)-\lambda^2\right]d\tau, \end{aligned} \tag{4}$$

valid for any regular stochastic point process, where $\lambda \equiv \mathrm{E}\{N[T]\}/T$ is the expected rate. Since the last relation of (4) is a new result, we provide its derivation in Appendix A. Reference [33] includes an example of how to derive the IDC using the first relation of (4) based on a two-state Markov-modulated Poisson process, the IDC of which was originally obtained by Heffes and Lucantoni [11].

### 2.3 Fractal nature of FPPs

The simplicity of our point process formulation lies in the fact that the four statistics CR, IDC, PSD, and COV in (4) are completely determined by each other. For fractal point processes

with a fractal exponent $\alpha$ (simply related to Hurst parameter $H$ by $\alpha = 2H - 1$) in the range $0 < \alpha < 1$, the second-order statistics will have special forms, and in the case of a *purely* fractal process[2] all of the following relationships hold [22]:

$$\begin{array}{lll} \text{CR:} & G(\tau)/\lambda^2 & = 1 + (|\tau|/\tau_0)^{\alpha-1} + \delta(\tau)/\lambda \\ \text{PSD:} & P(\omega)/\lambda & = 1 + (|\omega|/\omega_0)^{-\alpha} + \lambda\delta(\omega/2\pi) \\ \text{IDC:} & F(T) & = 1 + (T/T_0)^{\alpha} \\ \text{COV:} & C(k;T) & = \lambda T \cdot \begin{cases} 1 + (T/T_0)^{\alpha} & k = 0, \\ (T/T_0)^{\alpha}\nabla^2(k^{\alpha+1})/2 & k > 0, \end{cases} \end{array} \tag{5}$$

with

$$\begin{aligned} \omega_0^{\alpha} T_0^{\alpha} &= \cos(\pi\alpha/2)\Gamma(\alpha+2) \\ \lambda\tau_0^{1-\alpha} T_0^{\alpha} &= \alpha(\alpha+1)/2, \end{aligned} \tag{6}$$

where $\delta(x)$ is the Dirac delta function, $\nabla^2(\cdot)$ is the second central difference operator

$$\nabla^2[f(k)] \equiv f(k+1) - 2f(k) + f(k-1),$$

and $\Gamma(x)$ is the (complete) gamma function

$$\Gamma(x) \equiv \int_0^{\infty} e^{-t} t^{x-1}\, dt.$$

The three constants $\tau_0, \omega_0$, and $T_0$ mark the lower or upper limits for significant scaling behavior in the CR, PSD, and IDC, respectively. The CR, PSD, IDC, and COV in (5) may be obtained from each other through (4). The COV of (5) directly implies that the (normalized) autocovariance function (ACF) $r(k;T)$ is given by

$$\begin{aligned} r(k;T) &\equiv C(k;T)/C(0;T) \\ &= \frac{T^{\alpha}}{T^{\alpha} + T_0^{\alpha}} \frac{1}{2} \nabla^2(k^{\alpha+1}) \qquad (k > 0), \end{aligned} \tag{7}$$

making the process $X = \{X_n\}$ long-range dependent. See Appendix A for a detailed proof.

For very small $T$, i.e. $T \ll T_0$, the prefactor $g(T) \equiv T^{\alpha}/(T^{\alpha} + T_0^{\alpha})$ in (7) approaches zero, so that the LRD property becomes negligible at this time scale. For large values of $T$, on the other hand, $g(T)$ approaches unity, showing that the process $X$ is long-range dependent. Broadly speaking, the time $T_0$ marks the lower limit for significant scaling behavior in the IDC and ACF. For this reason, we call this parameter the *fractal onset time*.

We note that a purely fractal process, one which exhibits scaling over *all* time and frequency ranges as in (5), presents mathematical difficulties; these processes have infinite power, for example. This difficulty is obviated in practice by restricting the validity of (5) to a finite range of times and frequencies, which must be the case for all measured packet traces. In this case, if any one of the relationships in (5) holds over the relevant time and frequency ranges

[2] A purely fractal point process is an abstraction for which all the relationships in (5) hold over the entire range of time and frequency scales.

then the other three must also, with the parameters again given by (6). Thus for fractal point processes all the second-order statistics exhibit power-law scaling with closely related exponents and constants. This means that for $0 < \alpha < 1$ and over the specified ranges, three parameters suffice to specify the second-order statistics of a fractal point process: the mean rate $\lambda$, the fractal exponent $\alpha$, and the fractal onset time $T_0$. [Equivalently, either $\omega_0$ and $\tau_0$ can be specified instead of $T_0$, since any one specifies the other two via (6).] Further, FPPs produce asymptotically (second-order) self-similar processes for fractal exponents in the range $0 < \alpha < 1$, as we now show.

Recall that $X_n$ represents the number of arrivals in the $n$th counting window of duration $T$. Since

$$X_n^{(m)} \equiv m^{-1} \sum_{i=(n-1)m+1}^{nm} X_i$$

is formed from $X_n$ by concatenating adjacent counting intervals, we have

$$C^{(m)}(k;T) = m^{-2} C(k;mT),$$

yielding

$$r^{(m)}(k;T) = r(k;mT). \tag{8}$$

Combining (7) and (8) results in

$$r^{(m)}(k;T) = \frac{(mT)^\alpha}{T_0^\alpha + (mT)^\alpha} \frac{1}{2} \nabla^2(|k|^{\alpha+1}), \tag{9}$$

so that

$$\lim_{m\to\infty} r^{(m)}(k;T) = \frac{1}{2}\nabla^2(|k|^{\alpha+1}).$$

Thus, the process $X$ exhibits asymptotically second-order self-similarity [4]. In addition, since $C^{(m)}(0;T) = \mathrm{Var}(X^{(m)})$, we have

$$\mathrm{Var}(X^{(m)}) = \lambda T \left[ m^{-1} + (T/T_0)^\alpha m^{-(1-\alpha)} \right],$$

indicating that the variance of $X^{(m)}$ varies as $\sim m^{-(1-\alpha)}$ for large $m$. Thus the process $X$ also has the slowly-decaying variance property, another mathematically equivalent manifestation of self-similarity [4]. Therefore, the discrete-time process $X = \{X_n, n = 1, 2, \ldots\}$ constructed with an FPP and with $0 < \alpha < 1$ is asymptotically second-order self-similar with Hurst parameter $H = (\alpha + 1)/2$.

## 3 TWO FPP CONSTRUCTION METHODS

We employ the coincidence rate as a starting point since it is convenient and equivalent to the other second-order statistics of interest, as indicated in (4). By the argument of Section 2.3, any point process with a CR following the form of (5) will yield a (second-order) self-similar process. Two simple and effective methods are provided below which produce a point process whose CR is in the form of (5) and which is therefore a fractal point process.

### 3.1 Renewal point process method

A renewal point process by definition has interarrival times which are independent and identically distributed; thus the interarrival time pdf completely specifies this process. If the pdf is heavy tailed, then the coincidence rate $G(\tau)$ will also decay in a power law form, as given by (5) [21]; this yields the fractal renewal point process (Section 4). The superposition of a number of independent and identical realizations of this process also has a coincidence rate of the same form, and therefore also belongs to the fractal point process family (Section 5). Since the behavior of the tail of the interarrival time pdf determines the power-law form of the CR and hence the fractal nature of the fractal point process, the behavior of the interarrival time pdf at short times is arbitrary. Thus a wide variety of renewal-based fractal point processes exist for a given average rate $\lambda$ and power-law exponent $\alpha$.

### 3.2 Doubly stochastic Poisson process method

The doubly stochastic Poisson point process (DSPP) method derives from the similarity between the CR of a DSPP and autocorrelation function of its input rate process. To show this, let $I(t)$ denote the stationary stochastic input rate process of a DSPP, and $R_I(\tau)$ denote the autocorrelation function of this rate process, i.e., $R_I(\tau) \equiv \mathrm{E}[I(0)I(\tau)]$. Then, for $\tau \neq 0$ we have

$$\begin{aligned}
G(\tau) &\equiv \lim_{\Delta\to 0} \frac{\Pr\{\mathcal{E}(0,\Delta) \text{ and } \mathcal{E}(\tau,\tau+\Delta)\}}{\Delta^2}, \\
&= \lim_{\Delta\to 0} \frac{\mathrm{E}\left[\Pr\{\mathcal{E}(0,\Delta) \text{ and } \mathcal{E}(\tau,\tau+\Delta)\}|\ I(t)\right]}{\Delta^2} \\
&= \lim_{\Delta\to 0} \frac{\mathrm{E}\left[\Pr\{\mathcal{E}(0,\Delta) \text{ and } \mathcal{E}(\tau,\tau+\Delta)\}|\ I(0), I(\tau)\right]}{\Delta^2} \\
&= \lim_{\Delta\to 0} \mathrm{E}\left[\frac{\left\{1-\exp[-\int_0^{\Delta} I(u)du]\right\}\left\{1-\exp[-\int_{\tau}^{\tau+\Delta} I(v)dv]\right\}}{\Delta^2}\right] \\
&= \lim_{\Delta\to 0} \mathrm{E}\left[\frac{\{1-\exp[-I(0)\Delta]\}\{1-\exp[-I(\tau)\Delta]\}}{\Delta^2}\right] \\
&= \lim_{\Delta\to 0} \mathrm{E}\left[\frac{I(0)\Delta I(\tau)\Delta}{\Delta^2}\right] \\
&= \lim_{\Delta\to 0} \mathrm{E}[I(0)I(\tau)] \\
&= R_I(\tau).
\end{aligned}$$

Using the fact that $\mathrm{E}\{[dN(t)]^2\} = \mathrm{E}[dN(t)]$ [1, p. 265], we have

$$G(\tau) = R_I(\tau) + \lambda\delta(\tau). \tag{10}$$

Thus if a stationary continuous-time stochastic process $I(t)$ with an autocorrelation function $R_I(\tau)$ having a power-law decaying form serves as the rate for a DSPP, the result will follow the form of (10) and therefore be a fractal point process. In the following we consider two

such fractal rate processes: fractal Binomial noise (FBN) and fractal shot noise (FSN). FBN consists of the superposition of several independent and identical fractal ON/OFF processes whose sojourn times are heavy-tailed (Section 6). FSN is a type of shot noise [27] where the linear filter assumes a power-law decaying form (Section 7).

We provide details of these four fractal point process models, which may be employed for characterizing self-similar network traffic. For each model we first identify the relevant parameters, then analyze how these parameters determine the three fundamental quantities ($\lambda$, $H$, $T_0$). In particular, we determine whether all three of these quantities can be independently specified. Finally, we consider the remaining parameters (those in excess of the three needed to specify $\lambda$, $H$, and $T_0$), if any, and their effects on the character of the fractal point process model. Such remaining parameters determine the statistics over short time scales and the clustering properties, for example. In fact, clustering over all (or a relatively large range of) time scales is a salient feature of FPPs; the details of this clustering, beyond that specified by $H$ alone, is expected to have a significant effect on queueing behavior, a subject of future study.

# 4 FRACTAL RENEWAL PROCESS

Perhaps the simplest fractal point process is the standard fractal renewal process [3], [16], [21], [23], [42]. For the standard FRP, the times between adjacent arrivals are independent random variables drawn from the same fractal pdf. This i.i.d. property limits the applicability of the FRP as a fractal network traffic model, since traces exhibit high correlation between packet (cell) arrivals. However, this model serves a good example of how a renewal point process can result in a (second-order) self-similar process. Fig. 1-(a) provides a schematic representation of this point process, for which the pdf decays as a power law

$$p_2(t) = \begin{cases} kt^{-(\gamma+1)} & \text{for } A < t < B, \\ 0 & \text{otherwise,} \end{cases} \tag{11}$$

where $A$ and $B$ are cutoff parameters, $\gamma$ is a fractal exponent ($0 < \gamma < 2$), and $k$ is a normalizing constant determined by the requirement $\int_0^\infty p_2(t)\,dt = 1$.

For $0 < \gamma < 1$ this process is fully fractal: the power spectral density, coincidence rate, index of dispersion for counts, and even the interarrival time pdf all exhibit power-law scaling as in (5) over time scales lying between $A$ and $B$, and with related power-law exponents completely determined by $\alpha = \gamma$. For $1 < \gamma < 2$ the PSD, IDC, CR, and ACF (but not the interarrival time pdf) still exhibit power-law scaling of the form of (5), but with an associated exponent given by $\alpha = 2 - \gamma$. For larger values of $\gamma$ the process no longer has fractal second order statistics. Thus $\alpha$ is limited to a range between zero and unity, and for each value of $\alpha$ there corresponds two values of $\gamma$. In practice, however, the range $1 < \gamma < 2$ proves superior for modeling network traffic. For $0 < \gamma < 1$ the resulting simulations are extremely bursty, unlike traffic data, and sample statistics do not reliably follow the analytic forms of (5) except for prohibitively large simulation lengths. Another advantage of employing $\gamma > 1$ is that it renders the outer cutoff $B$ unnecessary; setting $B \to \infty$ still leads to a positive mean rate, in contrast to the $\gamma < 1$ case. Eliminating the outer cutoff also yields better power-law behavior in the

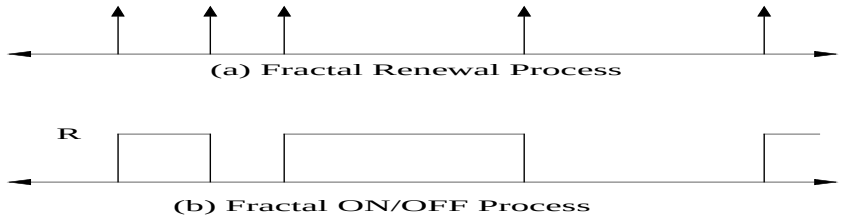


Figure 1: The standard fractal renewal process (FRP) and alternating FRP (fractal ON/OFF process) models. Interarrival times are power-law distributed. (a) The standard FRP consists of Dirac $\delta$ functions and is zero-valued elsewhere. (b) The alternating FRP (AFRP) switches between values of zero and $R$ ($> 0$).

PSD and IDC, and simplifies simulation [21]. The probability density function then assumes the simpler form

$$p_2(t) = \begin{cases} 0 & \text{for } t \leq A, \\ \gamma A^{\gamma} t^{-(\gamma+1)} & \text{for } t > A. \end{cases} \tag{12}$$

The form of the interarrival pdf in (12) can be further improved beyond choosing $\gamma$ in the range $1 < \gamma < 2$. For this pdf, the resulting IDC $F(T)$ exhibits a dip near $T = T_0$, caused by the abrupt cutoff in the interarrival time pdf that still remains; furthermore, the power spectral density exhibits excessive oscillations for the same reason. Improvement results from employing a smoother pdf [22]

$$p_2(t) = \begin{cases} \gamma A^{-1} e^{-\gamma t/A} & \text{for } t \leq A, \\ \gamma e^{-\gamma} A^{\gamma} t^{-(\gamma+1)} & \text{for } t > A, \end{cases} \tag{13}$$

which is continuous for all $t$. Other densities with support on the non-negative real line and with the same asymptotic properties exist such as $p_2(t) = \gamma A^{\gamma}(t+A)^{-(\gamma+1)}$ for $A > 0$. However, like the pdf in (12), these appear to lead to dips in the IDC.

The practical FRP model as presented in (13) has only two parameters: $\gamma$ and $A$. Thus this model cannot fully specify the set of fundamental quantities $\lambda$, $H$, and $T_0$, and only proves useful for simulating data with $\lambda T_0$ of the order of unity. Using the relation $\gamma = 2 - \alpha$ we obtain

$$\begin{aligned} H &= (\alpha+1)/2, \\ \lambda &= \gamma \left[1 + (\gamma-1)^{-1} e^{-\gamma}\right]^{-1} A^{-1}, \\ T_0^{\alpha} &= 2^{-1}\gamma^{-2}(\gamma-1)^{-1}(2-\gamma)(3-\gamma)e^{-\gamma}\left[1+(\gamma-1)e^{\gamma}\right]^2 A^{\alpha}. \end{aligned} \tag{14}$$

The procedure to obtain $T_0$ appears in [21].

## 5 SUPERPOSITION OF FRPs

A different fractal point process results from the superposition of a number of independent and identical FRPs. Although the resulting fractal point process (Sup-FRP) is no longer renewal, the marginal distribution of the interarrival times is still heavy-tailed (see Appendix B). Furthermore, the corresponding PSD, CR, IDC, and ACF retain their scaling behavior, albeit over a somewhat reduced range of times and frequencies. With each component FRP described by the interarrival time pdf given in (13), the number of parameters of the Sup-FRP increases to three: $\alpha$ and $A$ from the individual FRPs, and $M$, the number of FRPs superposed. In this case, the three fundamental quantities become [21]

$$\begin{aligned} H &= (\alpha+1)/2 \\ \lambda &= M\gamma\left[1+(\gamma-1)^{-1}e^{-\gamma}\right]^{-1}A^{-1}, \\ T_0^{\alpha} &= 2^{-1}\gamma^{-2}(\gamma-1)^{-1}(2-\gamma)(3-\gamma)e^{-\gamma}\left[1+(\gamma-1)e^{\gamma}\right]^{2}A^{\alpha}. \end{aligned} \tag{15}$$

with $\gamma = 2-\alpha$. The only difference between (15) and (14) is a factor of $M$ in the expression for $\lambda$; the quantities $H$ and $T_0$ remain unchanged. The Sup-FRP model indeed has three parameters, although $M$ can take only positive integer values. Thus arbitrary values of $\lambda$, $H$, and $T_0$ cannot be achieved exactly. In practice, we specify $\lambda$ and $H$, and adjust $M$ to approximate $T_0$ as closely as possible. The integer $M$ is of the order $\lambda T_0$; for most traffic data this quantity greatly exceeds unity, so that the finite resolution of $M$ does not pose a significant problem. If $X = \{X_k\}$ is constructed from this Sup-FRP, the marginal distribution of $X_k$ will approach a Gaussian form as $M \to \infty$ by the Central Limit Theorem since $\mathrm{E}[X_k^2] < \infty$ for finite $T$. In fact, for $\lambda T \gg 1$ the Gaussian approximation becomes quite accurate even with $M = 10$ [22]. This makes $X$ resemble the discrete-time fractional Gaussian noise (FGN) process [except for the factor of $T^{\alpha}/(T^{\alpha}+T_0^{\alpha})$ in the ACF], and thus the Sup-FRP becomes a computationally attractive alternative to generating the FGN process. This model has been successfully employed as a flexible, high-speed fractal ATM traffic generator on a real-time traffic generation and monitoring system built in Columbia University [33, Chap. 5].

## 6 FBNDP

The fractal renewal process (FRP) described previously is a point process, consisting of a set of points or marks on the time axis; however, it may be recast as a real-valued process which alternates between two values, such as zero and $R$ ($> 0$). This alternating fractal renewal process (AFRP) would then start at a value of zero ("OFF"), and then switch to a value of $R$ ("ON") at a time corresponding to the first event in the FRP. At the second such event in the FRP, the AFRP would switch back to zero, and would proceed to switch back and forth at every successive event of the FRP. Thus for the AFRP, all ON/OFF periods are i.i.d. with the same heavy-tailed distribution as in the FRP. Figure 1-(b) illustrates such a process.

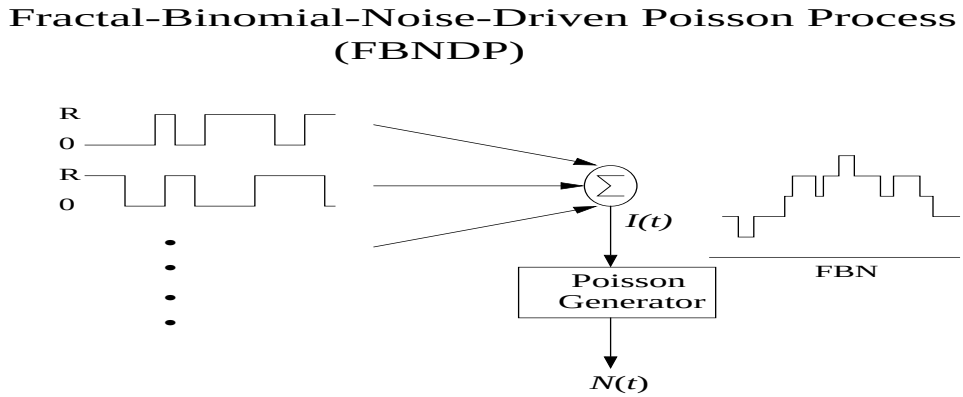


Figure 2: The FBNDP Model. A sum of $M$ i.i.d. AFRPs (left) are added (top center) to produce a fractal binomial noise process (right) which serves as the rate function for a Poisson point process (bottom). The result is the fractal-binomial-noise-driven Poisson point process (FBNDP), a fractal DSPP.

As with the Sup-FRP, $M$ i.i.d. AFRP processes may be added together, yielding fractal binomial noise (FBN) with the same fractal exponent as the single fractal ON/OFF process [21]. Let $I(t)$ denote the resulting FBN process. The autocorrelation function of $I(t)$ is merely a scaled version of the ACF of the individual AFRP processes, which in turn follows the decaying power-law form of (5) [21]. Thus $I(t)$ can serve as a stationary stochastic rate function for a Poisson process, resulting in the fractal-binomial-noise-driven Poisson point process (FBNDP) [22]. The construction of the FBNDP is schematized in Fig. 2.

Since $I(t)$ is a binomial process and the ON and OFF periods have identical mean values, we have

$$\Pr[I(t) = nR] = 2^{-M} \begin{pmatrix} M \\ n \end{pmatrix} = 2^{-M} \frac{M!}{n!(M-n)!} \tag{16}$$

for $n = 0, 1, 2, \ldots M$.

The FBNDP has four free parameters ($A$, $\alpha$, $R$, and $M$) which determine $\lambda$, $H$ and $T_0$ as follows, where we use (13) for the ON and OFF periods of the individual AFRP processes:

$$\begin{aligned} H &= (\alpha+1)/2, \\ \lambda &= RM/2, \\ T_0^\alpha &= \alpha(\alpha+1)(2-\alpha)^{-1}[(1-\alpha)e^{2-\alpha}+1]R^{-1}A^{\alpha-1}. \end{aligned} \tag{17}$$

See Appendix C for the derivation of $T_0$. Thus, ($\lambda$, $H$, $T_0$) can all be specified, leaving an extra parameter. This implies that different FBNDPs can be constructed with the same $\lambda$, $H$, and $T_0$. For example, decreasing $M$ (while increasing $R$ to keep the overall rate $\lambda$ constant) will increase the probability that the rate becomes zero [see (16)], during which no arrivals can occur. Since the OFF period is also heavy-tailed, the resulting FBNDP exhibits a high degree of clustering, especially for the limiting case $M = 1$. In this case, heavy-tailed periods of arrivals will alternate with heavy-tailed inter-burst quiescent periods. Similarly, increasing $M$ reduces clustering. Later, we will use this model to characterize aggregate Ethernet traffic collected at Bellcore. As with the Sup-FRP, the Central Limit Theorem again provides that the increments process $X$ constructed from this process will approach a fractional Gaussian noise process as $M \to \infty$.

## 7 FSNDP

The fractal-shot-noise-driven Poisson point process (FSNDP) [20] is another special case of the DSPP. For the FSNDP, the rate of the inhomogeneous Poisson process is fractal shot noise [17, 18, 19], which is itself a filtered version of a different, homogeneous Poisson point process. Figure 3 schematically illustrates the FSNDP as a two-stage stochastic process [39].

The first stage is a homogeneous Poisson process (HPP) with constant rate $\mu$. Its output $M(t)$ becomes the input to a linear filter with a power-law decaying impulse response function

$$h(t) = \begin{cases} c/t^{1-\alpha/2} & \text{for } A < t < B, \\ 0 & \text{otherwise,} \end{cases} \tag{18}$$

with $\alpha$, $A$, and $B$ defined as following (11), and $c$ a positive amplitude constant. This filter produces fractal shot noise $I(t)$ at its output, which then becomes the stochastic rate for the last stage, a second Poisson point process. The resulting point process is not homogeneous, but rather reflects the variations of the fractal-shot-noise driving process. Thus the two forms of randomness inherent in the DSPP are, in the particular case of the FSNDP, two separate Poisson processes, linked by a power-law-decaying linear filter. As a result of this filter, the FSNDP exhibits fractal behavior of the form of (5) for time scales in the range $A \ll T \ll B$.

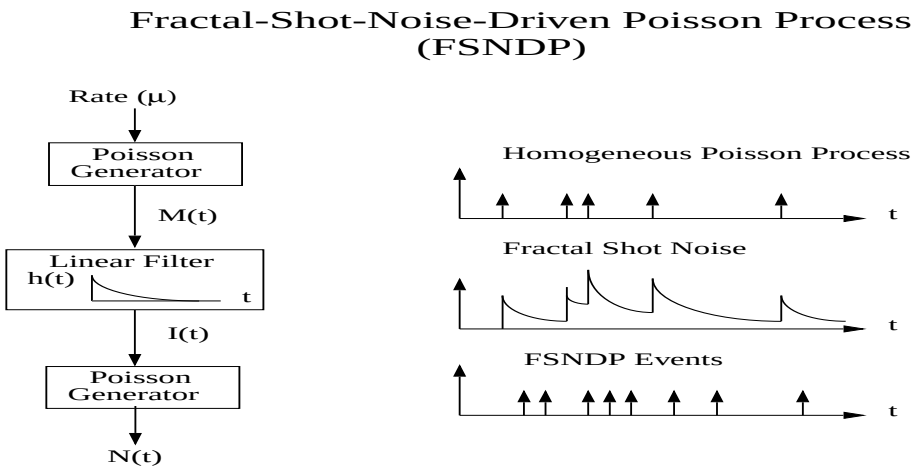


Figure 3: The FSNDP Model. The process $I(t)$ at the output of the filter is shot noise. If the impulse response function $h(t)$ decays in a power-law fashion, then $I(t)$ is fractal shot noise and $N(t)$ is an FSNDP process.

The FSNDP model has five parameters, $A$, $B$, $\alpha$, $c$, and $\mu$. For $A \ll T_0$ and $A \ll B$, they determine ($H$, $\lambda$, $T_0$) as follows [20]:

$$\begin{aligned} H &= (\alpha+1)/2 \\ \lambda &= 2\alpha^{-1}\mu c B^{\alpha/2} \\ T_0^{\alpha} &= \frac{\alpha(\alpha+1)\Gamma(1-\alpha/2)}{2\Gamma(1+\alpha/2)\Gamma(1-\alpha)} c^{-1} B^{\alpha/2}. \end{aligned} \tag{19}$$

Since $A$ does not appear in (19), in many applications it can be set to zero, which results in a rate function $I(t)$ with infinite variance. This proves not to be problematic, since an integrated version of the shot noise (which necessarily has a finite variance), is more directly involved in FSNDP statistics. Four parameters remain, so that as with the FBNDP a free parameter exists which determines the clustering characteristics of the process; we focus on the product $\mu B$. For small values of this quantity, successive impulse response functions rarely overlap, leading to large gaps between impulse response functions where FSNDP arrivals cannot occur.

In this case the process appears highly clustered. When $\mu B$ greatly exceeds unity, then the impulse response functions will overlap, eliminating the longer intervals. Indeed, in this limit (and with $A > 0$) the process $X$ constructed from the FSNDP will converge to the fractional Gaussian noise processes.

We note that the impulse response function $h(t)$ may be changed, for example, to time-symmetric forms or ones with more gradual cutoffs. Any form for $h(t)$ will yield fractal behavior as long as it varies as $1/t^{1-\alpha/2}$ for a significant range of times $t$, and $\mu \int_{-\infty}^{\infty} h(t)\, dt = \lambda$. However, forms other than the one proposed in (18) appear to complicate simulation. We further note that the height of the impulse response function $h(t)$, denoted by $c$ in (18), can also be random as long as it has finite first and second moments [20]; this further extends the range of fractal point processes.

The FSNDP model was first used for characterizing a point-to-point videoconferencing application exhibiting fractal behavior [36]. In the next section, we use this model to characterize external Ethernet traffic again collected at Bellcore.

# 8 PRACTICALITY OF FPPs: QUEUEING STUDY

In this section, two fractal point process models are used to characterize the two empirical data sets obtained from Bellcore: the FBNDP for the pAug trace, and the FSNDP for the OctExt trace, respectively[3].

We begin by analyzing these traces from a point process point of view. We extract packet arrival times from each of two traces, and treat the resulting time series as an arrival stream from a source. Table 1 shows the sample statistics of these two traces.

| | pAug | OctExt |
|---|---|---|
| Length | 3,150 (sec) | 122,800 (sec) |
| Packets | 1 million | 1 million |
| $\lambda$ | 318.2 (pkts/sec) | 8.1 (pkts/sec) |
| Peak rate | 838 (pkts/sec) | 1335 (pkts/10secs) |
| Peak-to-mean | 2.6 | 16.4 |
| $\alpha$ | 0.73 | 0.84 |
| $H$ | 0.87 | 0.92 |
| $T_0$ | 0.006 (sec) | 0.033 (sec) |

Table 1: Statistics of the two Bellcore traces.

Fig. 4 shows the sample paths of the two traces, which may be readily distinguished. The pAug looks somewhat regular due to the high aggregation level; the OctExt looks quite bursty, and perhaps non-stationary due to the low level of aggregation (being external traffic) and apparent daily cycle. The choice of the FBNDP model for the pAug trace was relatively easy since the theoretical peak-to-mean ratio of the FBNDP, $RM/\lambda$, is always equal to 2 (ignoring

[3]These traces, collected in 1989, are available at ftp.bellcore.com under the directory /pub/wel/lan-traffic.

the local Poisson variation); see (17). This agrees well with the peak-to-mean ratio of the trace pAug, which attains a value of 2.6 at a time scale of 1 sec. On the other hand, the activity of the OctExt trace differs significantly from On/Off-type behavior. For example, its peak-to-mean ratio is 16.4 at a time scale 10 sec. Further, the apparent non-stationarity renders the application of stationary models difficult. We choose the FSNDP model for the OctExt trace since it is flexible [37] and able to yield high peak-to-mean ratio; see Fig. 4. As will be shown later, the queueing behavior of both models agree well with that of the traces, showing the flexibility and wide applicability of the point process formulation.

To match the given fractal data, we use the following heuristic procedure to determine the parameters of the FBNDP and FSNDP models:

1. The average arrival rate $\lambda$ is obtained by dividing the number of total arrivals by the length of the trace in time.
2. $(H, T_0)$ are determined from the IDC curve $F(T)$ by a least-squares fit of $\log[F(T) - 1]$ vs. $\log T$ [36].
3. Once the three fundamental quantities are determined, trial values of the free parameters ($M$ for the FBNDP and $B$ for the FSNDP) are selected based on the detailed behavior of the target trace (such as clustering) or previous experience.
4. From $(\lambda, H, T_0)$ and the given free parameters, we obtain the model parameters using (17) and (19).
5. Models with these parameters are simulated.
6. Steps 3-5 are iterated until the detailed behavior of the models closely follow sample paths and queueing behavior of the empirical data.

We note that the method of determining the free parameters in the above procedure can be further refined to be more systematic. For instance, choosing the free parameter such that the autocorrelations (or marginal distributions) of the interarrival times of the trace and the model are closely matched is one possible method. However, such an approach still remains heuristic since both the autocorrelations and the marginal distributions of the interarrival times of the FBNDP and FSNDP models are not mathematically tractable [20]. As a result, finding a more systematic matching procedure requires extensive simulation of the FPP models with widely varying model parameters, a subject of further study.

| FBNDP | FSNDP |
|---|---|
| $A = 0.036$ (sec) | $\mu = 0.0005$ (sec$^{-1}$) |
| $R = 212.13$ (sec$^{-1}$) | $c = 171$ |
| $M = 3$ | $B = 5000$ (sec) |
| | $A = 0.0001$ (sec) |

Table 2: Parameters of the FBNDP and FSNDP models matched to the pAug and OctExt datasets, respectively.

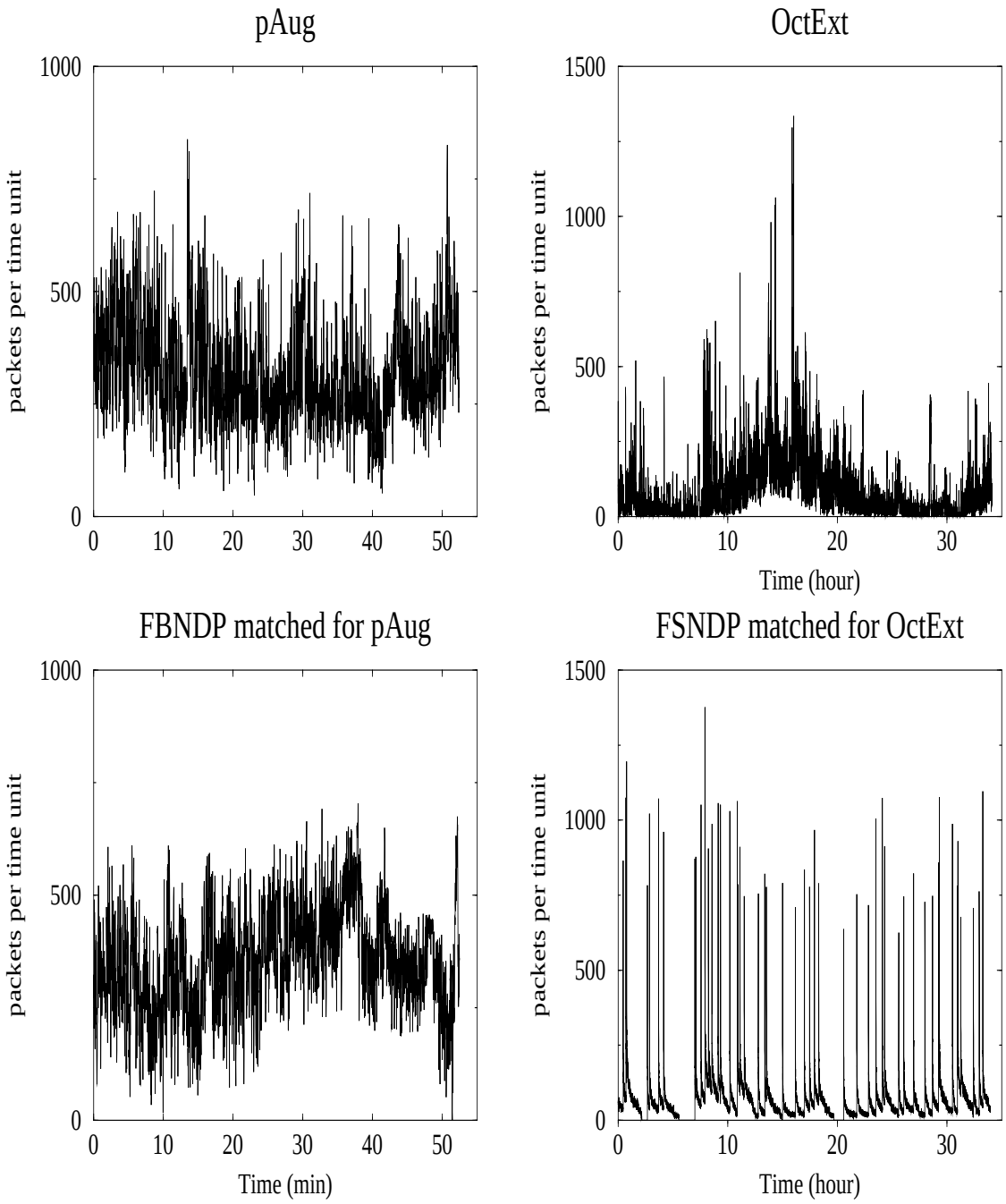


Figure 4: Sample paths of two traces and matched models in terms of packets per time unit (1 sec for pAug and FBNDP and 10 sec for OctExt and FSNDP). While the results of the FBNDP agrees closely with pAug, the FSNDP instantaneous rates differ from those of OctExt due to apparent non-stationarity in this dataset.

Table 2 shows the values of the model parameters resulting from the above matching procedure, and Fig. 5 shows the IDC curves of the traces and matched models. Note the close agreement between the trace and the models over a wide range of time scales.

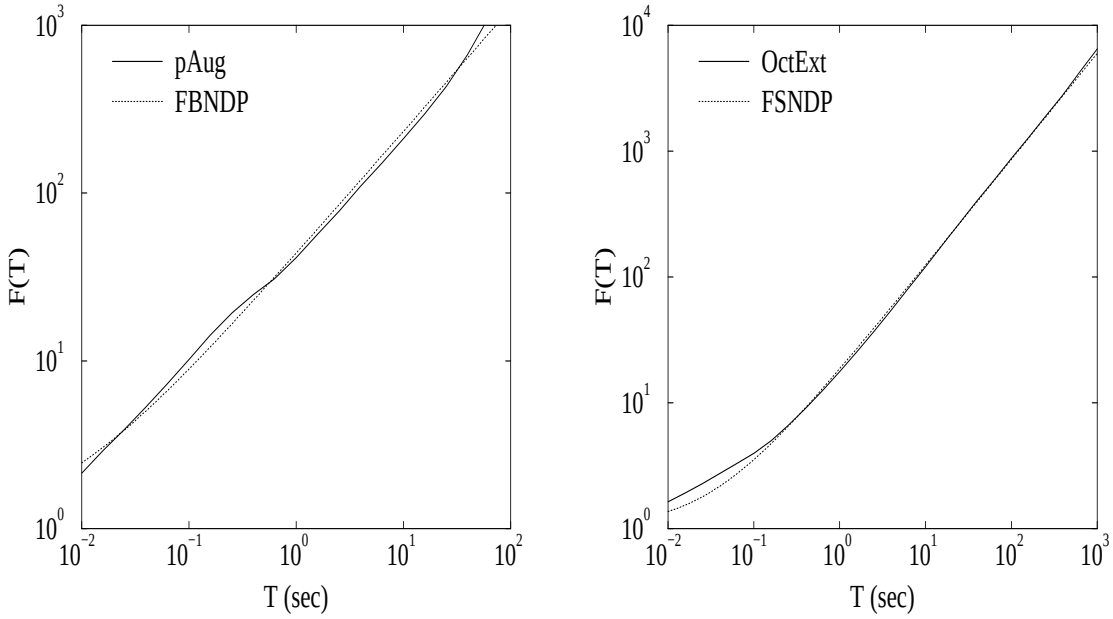


Figure 5: IDC curves of traces and matched models.

We next simulate a single-server queue with infinite waiting room and FIFO service discipline. We assume that each arrival brings an exponentially-distributed service requirement with a mean of 1000 bytes. Since our focus lies in the queueing behavior caused by randomness in an arrival process, the service requirement is not critical as long as that of both the trace and the model are identical. We therefore choose the exponential packet-size distribution to simplify the simulation.

For each trunk utilization level, we estimate the buffer overflow probability $\Pr(B > x)$ of the trace and that of the matched model. Figure 6 compares the trace-driven and model-driven simulation results. The sharp drop in the probabilities for large buffer sizes in Fig. 6 is due to insufficient data. While the FBNDP model shows excellent agreement with pAug, the FSNDP shows noticeable discrepancy from OctExt for small buffer size. We suspect that this arises from the different short-term correlations and rate distribution of the trace and the model, visible in the instantaneous rate in Fig. 4. We note that improvements of the FSNDP may be possible by allowing for randomness in the height $c$ of the impulse response function $h(t)$, which is under study. Queueing behavior at different utilization levels shows similar trends both quantitatively and qualitatively [33]. These results reveal the efficacy of our FPP models in evaluating the queueing performance of various types of real traffic sources exhibiting fractal behavior.

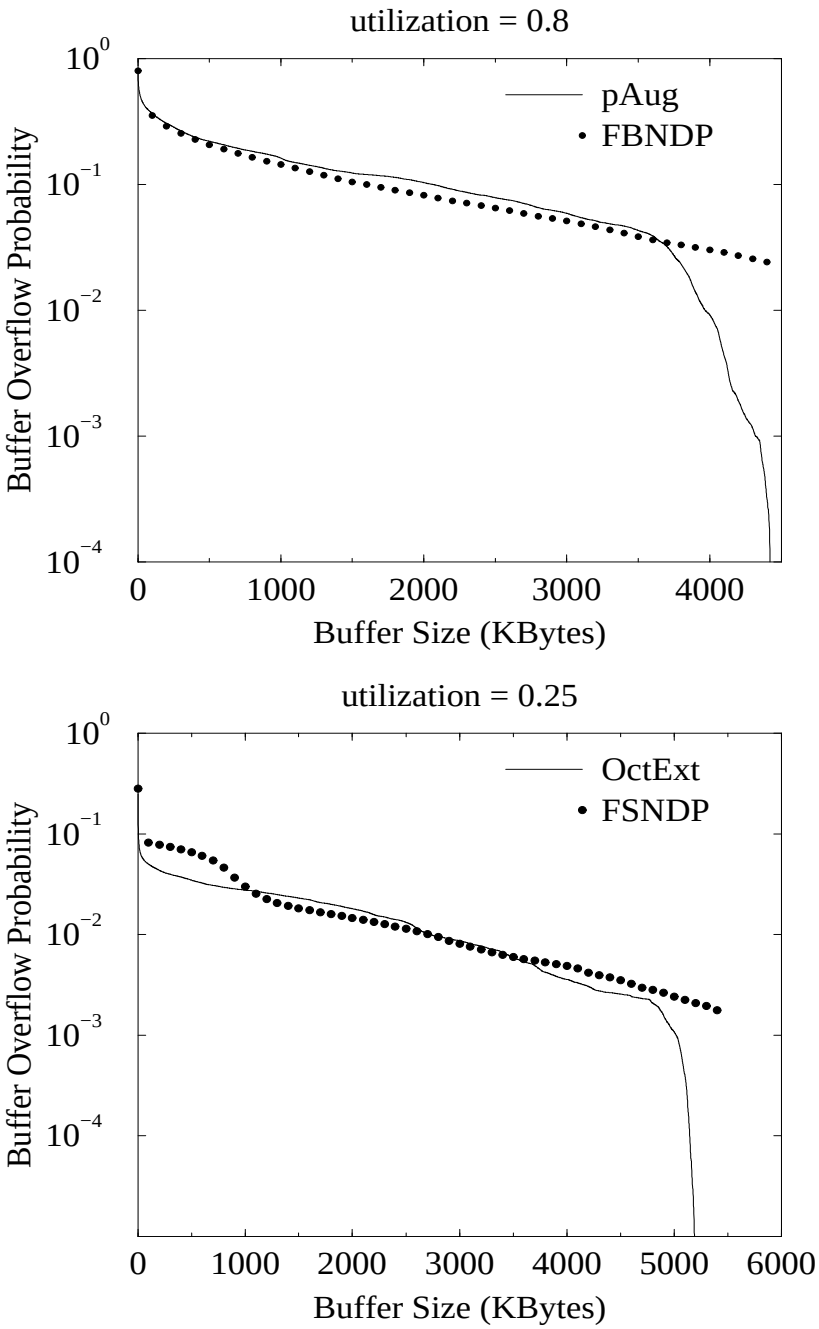


Figure 6: Comparison of the queueing behavior of the traces and matched models. Left: pAug and FBNDP, Right: OctExt and FSNDP.

## 9 Concluding Remarks

We have shown that the point process formulation provides two simple methods which yield parsimonious, computationally efficient [37], and diverse types of self-similar models based on fractal point processes. Self-similar processes based on FPPs prove useful since many fractal characteristics are inherent in FPPs and therefore are automatically included in the resulting self-similar processes. Using this framework, we have shown that the relevant second-order fractal characteristics such as long-range dependence, slowly decaying variance, and $1/f$ noise, are completely characterized by three fundamental quantities. Four models have been proposed, and the relationship between their model parameters and the three fundamental quantities have been analyzed. In particular, we have examined how the free parameter(s) affect the detailed behavior of the process, which may lead to different queueing performance with the same second-order fractal characteristics (and thus same three fundamental quantities).

In the context of network performance, we have also shown that our fractal point process models are able to capture the queueing behavior of fractal traces under a wide range of buffer sizes, proving the usefulness of the FPP models in evaluating and predicting queueing performance of fractal traffic sources. Indeed, the types of fractal behavior manifested in real fractal traces appear to be much more diverse than those of previous models proposed in the literature. In order to investigate the realistic impact of traffic bearing fractal characteristics on the design and control of future high-speed networks, it is critical to employ practical rather than abstract models. This work clearly indicates that fractal process models will prove useful in this sense. The popularity of the Internet, with its traffic exhibiting strong statistical evidence of fractal behavior [29], makes an FPP approach promising, mathematical, and highly practical for understanding extreme variability of current packet network traffic.

## Acknowledgments

Part of this work was completed while the first author was on leave with Bell Laboratories, Murray Hill, New Jersey. He is grateful to Anwar Elwalid and Debasis Mitra for their encouragement and support. The authors are also grateful to the three anonymous referees for their constructive comments which greatly improved the presentation of this paper.

## Appendix A: Long-Range dependence of FPPs

Define $N(t)$ as the number of arrivals of a stationary stochastic point process occurring between the origin and a specified time $t$. Let $\lambda$ denote the mean rate of the process, so that $\mathrm{E}[N(t)] = \lambda t$ for all $t$. Denote by $N(t,s]$ the number of arrivals during the interval $(t,s]$, i.e., $N(t,s] \equiv N(s) - N(t)$. Then from the definition of $C(k;T)$ given by (3), we have

$$\begin{aligned} C(k;T) &= \mathrm{E}\left\{N(0,T]N(kT,(k+1)T]\right\} - \mathrm{E}^2\left\{N(0,T]\right\} \\ &= \mathrm{E}\left[\int_0^T dN(t)\int_{kT}^{(k+1)T} dN(s)\right] - (\lambda T)^2 \end{aligned}$$

$$
\begin{aligned}
&= \int_0^T \int_{kT}^{(k+1)T} \mathrm{E}\left[dN(t)dN(s)\right] - (\lambda T)^2 \\
&= \int_0^T \int_{kT}^{(k+1)T} G(t-s)\, dtds - (\lambda T)^2 \\
&= \int_{-T}^{T} (T-|\tau|) G(kT+\tau)\, d\tau - (\lambda T)^2 \\
&= \int_{-T}^{T} (T-|\tau|)[G(kT+\tau) - \lambda^2]\, d\tau \qquad (20)
\end{aligned}
$$

where the fourth equality follows from (2). For a stationary FPP, $G(\tau)$ is given by (5); substituting this into (20) and using the second line of (6) results in

$$
C(k;T) = \begin{cases} \lambda T[1 + (T/T_0)^\alpha] & \text{for } k = 0 \\ \lambda T (T/T_0)^\alpha \frac{1}{2} \nabla^2 (k^{\alpha+1}) & \text{for } k = 1, 2, 3, \ldots \end{cases}
$$

which completes the proof.

## Appendix B: Time Statistics for Superpositions of Fractal Renewal Point processes (Sup-FRP)

Consider a general renewal point process, with an average interarrival time $\langle T \rangle$, interarrival time probability density function IPDF $p_2(t)$, and associated survivor function $S_2(t) \equiv \Pr\{T > t\} = \int_t^\infty p_2(u)\, du$. The forward recurrence time probability density function FPDF is given by $p_1(t) = \langle T \rangle^{-1} S_2(t)$, and has a survivor function $S_1(t)$, which is equal to the probability that there will be no arrivals in the renewal process during a period of duration $t$ which starts at a random time independent of the process. This survivor function is given by

$$
\begin{aligned}
S_1(t) &= \int_t^\infty p_1(u)\, du = \langle T \rangle^{-1} \int_t^\infty S_2(u)\, du \\
&= \langle T \rangle^{-1} \int_{u=t}^\infty \int_{v=u}^\infty p_2(v)\, dvdu = \langle T \rangle^{-1} \int_t^\infty (v-t) p_2(v)\, dv.
\end{aligned}
$$

For $M$ independent identical renewal point processes, the probability of no events occurring in any of the $M$ processes in a time $t$ is merely the product of the probabilities from the individual processes. We denote statistics of this aggregated process by the subscript $M$. Therefore the forward recurrence survivor function for the aggregate process $S_{M1}$ becomes

$$
S_{M1}(t) = S_1^M(t) = \langle T \rangle^{-M} \left[ \int_t^\infty (v-t) p_2(v)\, dv \right]^M,
$$

while taking the derivative with respect to time yields the forward recurrence time probability density function,

$$
p_{M1}(t) = M \langle T \rangle^{-M} \left[ \int_t^\infty (v-t) p_2(v)\, dv \right]^{M-1} \int_t^\infty p_2(v)\, dv.
$$

Multiplying by the average interarrival time $\langle T\rangle/M$ of the aggregate process yields the interarrival time survivor function:

$$S_{M2}(t) = \langle T\rangle^{-(M-1)} \left[\int_t^\infty (v-t)p_2(v)\,dv\right]^{M-1} \int_t^\infty p_2(v)\,dv,$$

while another differentiation yields the interarrival time probability density function

$$\begin{aligned} p_{M2}(t) &= \langle T\rangle^{-(M-1)} \left[\int_t^\infty (v-t)p_2(v)\,dv\right]^{M-2} \\ &\times \left\{(M-1)\left[\int_t^\infty p_2(v)\,dv\right]^2 + p_2(t)\int_t^\infty (v-t)p_2(v)\,dv\right\}. \end{aligned}$$

Now consider the particular case of a single fractal renewal point process with abrupt cutoffs, where the interarrival time probability density function assumes the form

$$p_2(t) = \frac{\gamma}{A^{-\gamma}-B^{-\gamma}} \begin{cases} t^{-(\gamma+1)} & \text{for } A<t<B \\ 0 & \text{otherwise,} \end{cases}$$

with $0<\gamma<2$ and $0<A\ll B$. The average interarrival time then becomes

$$\langle T\rangle = \begin{cases} \dfrac{\gamma}{1-\gamma}\dfrac{B^{1-\gamma}-A^{1-\gamma}}{A^{-\gamma}-B^{-\gamma}} & \text{for } 0<\gamma<1, \\[2ex] \dfrac{AB}{B-A}\ln(B/A) & \text{for } \gamma=1, \\[2ex] \dfrac{\gamma}{\gamma-1}\dfrac{A^{1-\gamma}-B^{1-\gamma}}{A^{-\gamma}-B^{-\gamma}} & \text{for } \gamma>1. \end{cases}$$

If $t<A$, then $p_2(t)=0$, and $S_2(t)=1$, so $p_1(t)=\langle T\rangle^{-1}$ and $S_1(t)=1-t/\langle T\rangle$. For very small times such that $t\ll A$, we then have

$$S_{M1}(t) = S_1^M(t) = (1-t/\langle T\rangle)^M \approx 1-Mt/\langle T\rangle \approx \exp\left(-Mt/\langle T\rangle\right), \tag{21}$$

the same result as for a homogeneous Poisson process (HPP) with identical rate. Thus for very short time scales, the time statistics of superpositions of independent, identically distributed FRPs behave like those of HPPs. For long times $t$ where $t>B$, both probability density functions and both survivor functions reach a value of zero, which therefore also holds for superpositions.

Lastly we consider the range $A\ll t\ll B$, where the statistics depend explicitly on $\gamma$. For $0<\gamma<1$ we have

$$S_1(t) \approx (1-\gamma)B^{\gamma-1}\int_t^B (v-t)v^{-(\gamma+1)}\,dv \approx 1-\gamma^{-1}(t/B)^{1-\gamma},$$

so that

$$S_{M1}(t) \approx \left[1-\gamma^{-1}(t/B)^{1-\gamma}\right]^M \approx 1-(M/\gamma)(t/B)^{1-\gamma}$$

for $A \ll t \ll B/M^{1/(1-\gamma)}$. Therefore, for $0 < \gamma < 1$ and this range of $t$, the time statistics for the superposed FRP resemble those of a single FRP. In this case, many such FRPs will be required before the superposition approaches a Poisson form, on the order of $M = (B/A)^{1-\gamma}$. Indeed, the IPDF for the superposed process becomes

$$p_{M2}(t) \approx \gamma A^{\gamma} t^{-(\gamma+1)} = p_2(t);$$

since each FRP is so sparse for this range of $\gamma$, superposing several of them does not change the time statistics appreciably.

For $\gamma = 1$ and $A \ll t \ll B$ we have

$$\begin{aligned} S_1(t) &= \ln^{-1}(B/A) \int_t^B (v-t)v^{-2}\, dv \approx \frac{\ln(B/t)}{\ln(B/A)} \\ S_{M1}(t) &\approx \frac{\ln^M(B/t)}{\ln^M(B/A)}, \end{aligned}$$

so again only for many FRPs will the superposition resemble a Poisson process.

For $\gamma > 1$ and $A \ll t \ll B$, fewer FRPs are required. We have for this range of parameters

$$\begin{aligned} S_1(t) &\approx \gamma^{-1}(t/A)^{1-\gamma} \\ S_{M1}(t) &\approx \gamma^{-M}(t/A)^{M(1-\gamma)}, \end{aligned}$$

so that the survivor function of the superposition decays progressively faster as more FRPs are added, approaching the exponential limit of the Poisson process much more quickly than for $0 < \gamma < 1$.

## Appendix C: Fractal Onset Time of the FBNDP

Denote by $I(t)$ the superposition of $M$ i.i.d. alternating fractal renewal processes (AFRPs) defined by (13), which yields fractal Binomial noise. Let $I(t)$ drive a Poisson generator (see Fig. 2). We easily obtain $\lambda = \mathrm{E}[I(t)] = RM/2$ [20]. To derive $T_0$, we start with $M = 1$ and $R = 1$. The PSD of $I(t)$, $P_I(\omega)$, is given by

$$P_I(\omega) \approx 2^{-1}(2-\alpha)\Gamma(\alpha)\cos(\pi\alpha/2)[(1-\alpha)e^{2-\alpha}+1]^{-1}A^{1-\alpha}\omega^{-\alpha} \tag{22}$$

for $0 < \omega \ll A^{-1}$ and $0 < \alpha < 1$. Let $I(t)$ be used as a rate function for a Poisson point process denoted by $dN(t)$. In the general case of $R \neq 1$, the PSD of $dN(t)$, denoted by $P_N(\omega)$, may be obtained from $P_I(\omega)$ by multiplying $R^2$ and adding the average rate of the Poisson process, equal to $R/2$ [1]. This yields

$$P_N(\omega) = R^2 P_I(\omega) + R/2.$$

Finally, we consider $M$ AFRPs. Since they are i.i.d., their PSDs add, resulting in

$$\begin{aligned} P_N(\omega) &= MR^2 P_I(\omega) + MR/2 \\ &\approx 2^{-1}(2-\alpha)MR^2\Gamma(\alpha)\cos(\pi\alpha/2)[(1-\alpha)e^{2-\alpha}+1]^{-1}A^{1-\alpha}\omega^{-\alpha} \\ &\quad + MR/2. \end{aligned} \tag{23}$$

To find $\omega_0$, we set the two terms in (23) equal to each other since $P_N(\omega_0) = 2\lambda = MR$ [see (5)]. The factor of $M$ cancels, yielding

$$\omega_0^\alpha = \frac{(2-\alpha)\Gamma(\alpha)\cos(\pi\alpha/2)}{(1-\alpha)e^{2-\alpha}+1} RA^{1-\alpha}. \tag{24}$$

In combination with the first line of (6), this yields

$$T_0^\alpha = \alpha(\alpha+1)(2-\alpha)^{-1}\left[(1-\alpha)e^{2-\alpha}+1\right] R^{-1}A^{\alpha-1}.$$

## References


[1] Bartlett, M. The spectral analysis of point process. *J. Roy. Stat. Soc. B*, 25(2):264–296, 1963.

[2] Beran, J., Sherman, R., Taqqu, M. S., and Willinger, W. Long-range dependence in variable-bit-rate video traffic. *IEEE Trans. Comm.*, 43:1566–1579, 1995.

[3] Berger, J. M. and Mandelbrot, B. B. A new model for the clustering of errors on telephone circuits. *IBM J. Res. Dev.*, 7:224–236, 1963.

[4] Cox, D. R. Long-range dependence: A review. In H. A. David and H. T. Davis, editors, *Statistics: An Appraisal*, pages 55–74. The Iowa State University Press, Ames, Iowa, 1984.

[5] Cox, D. R. and Lewis, P. A. W. *The Statistical Analysis of Series of Events*. Methuen, London, 1966.

[6] Duffield, N. G., Lewis, J. T., and O'Connell, N. Predicting Quality of Service for traffic with long-range fluctuations. In *Proc. ICC*, Seattle, WA, 1995.

[7] Erramilli, A., Narayan, O., and Willinger, W. Experimental queueing analysis with long-range dependent packet traffic. *IEEE/ACM Trans. Net.*, 4:209–223, 1996.

[8] Erramilli, A., Singh, R. P., and Pruthi, P. An application of deterministic chaotic maps to model packet traffic. *Queueing Systems*, 20:171–206, 1995.

[9] Fowler, H. J. and Leland, W. E. Local area network traffic characteristics, with implications for broadband network congestion management. *IEEE JSAC*, 9:1139–1149, 1991.

[10] Garrett, M. W. and Willinger, W. Analysis, modeling and generation of self-similar VBR video traffic. In *Proc. ACM SIGCOMM*, London, England, 1994.

[11] Heffes, H. and Lucantoni, D. M. A Markov modulated characterization of packetized voice and data traffic and related statistical multiplexer performance. *IEEE JSAC*, SAC-4(6):856–868, September 1986.

[12] Heyman, D. P. and Lakshman, T. V. What are the implications of long-range dependence for VBR-video traffic engineering? To appear in *IEEE/ACM Trans. Net.*, 1996.

[13] Leland, W. E. et al. On the self-similar nature of Ethernet traffic (extended version). *IEEE/ACM Trans. Net.*, 2:1–15, 1994.

[14] Likhanov, N., Tsybakov, B., and Georganas, N. D. Analysis of an ATM buffer with self-similar ("fractal") input traffic. In *Proc. IEEE INFOCOM*, Boston, MA, 1995.

[15] Lowen, S. B. Fractal renewal processes as a model of charge transport in amorphous semiconductors. *Phys. Rev. B*, 46:1816–1819, 1992.

[16] Lowen, S. B. *Fractal Stochastic Processes.* PhD thesis, Columbia University, 1992.

[17] Lowen, S. B. and Teich, M. C. Fractal shot noise. *Phys. Rev. Lett.*, 63:1755–1759, 1989.

[18] Lowen, S. B. and Teich, M. C. Generalized $1/f$ shot noise. *Electron. Lett.*, 25:1072–1074, 1989.

[19] Lowen, S. B. and Teich, M. C. Power-law shot noise. *IEEE Trans. Inf. Th.*, 36:1302–1318, 1990.

[20] Lowen, S. B. and Teich, M. C. Doubly stochastic Poisson point process driven by fractal shot noise. *Phy. Rev. A*, 43:4192–4215, 1991.

[21] Lowen, S. B. and Teich, M. C. Fractal renewal processes generate 1/f noise. *Phy. Rev. E*, 47:992–1001, 1993.

[22] Lowen, S. B. and Teich, M. C. Estimation and simulation of fractal stochastic point processes. *Fractals*, 3:183–210, 1995.

[23] Mandelbrot, B. B. Self-similar error clusters in communication systems and the concept of conditional stationarity. *IEEE Trans. Comm. Tech.*, 13:71–90, 1965.

[24] Mandelbrot, B. B. *The Fractal Geometry of Nature.* W. H. Freeman, 1982.

[25] Norros, I. A storage model with self-similar input. *Queueing Systems*, 16:387–396, 1994.

[26] Norros, I. On the use of fractional Brownian motion in the theory of connectionless networks. *IEEE JSAC*, 13:953–962, 1995.

[27] Papoulis, A. *Probability, Random Variables, and Stochastic Processes.* McGraw-Hill, New York, third edition, 1990.

[28] Parulekar, M. and Makowski, A. M. Buffer overflow probabilities for a multiplexer with self-similar input. In *Proc. IEEE INFOCOM*, San Francisco, CA, 1996.

[29] Paxson, V. An introduction to Internet measurement and modeling. *ACM SIGCOMM'96 Tutorial*, Stanford, CA, 1996.

[30] Paxson, V. and Floyd, S. Wide Area Traffic: the failure of Poisson modeling. *IEEE Trans. Net.*, 3:226–244, 1995.

[31] Pruthi, P. and Erramilli, A. Heavy-tailed On/Off source behavior and self-similarity. In *Proc. ICC*, Seattle, WA, 1995.

[32] Robert, S. and LeBoudec, J.-Y. Can Self-Similar traffic be modeled by Markovian processes? In B. Plattner, editor, *Lecture Notes in Comp. Sci. (Proc. Int'l Zurich Seminar on Dig. Comm.)*, volume 1044. Springer-Verlag, 1996.

[33] Ryu, B. K. *Fractal Network Traffic: From Understanding to Implications*. PhD thesis, Columbia University, 1996.

[34] Ryu, B. K. Implications of self-similarity for providing QOS guarantees end-to-end in high-speed networks: A framework of Application Level Traffic Modeling. In B. Plattner, editor, *Lecture Notes in Comp. Sci. (Proc. Int'l Zurich Seminar on Dig. Comm.)*, volume 1044, Zurich, Switzerland, 1996. Springer-Verlag.

[35] Ryu, B. K. and Elwalid, A. The importance of Long-Range Dependence of VBR video traffic in ATM traffic engineering: Myths and realities. In *Proc. ACM SIGCOMM*, San Francisco, CA, 1996.

[36] Ryu, B. K. and Lowen, S. B. Modeling, analysis, and generation of self-similar traffic with the Fractal-Shot-Noise-Driven Poisson process. In *Proc. IASTED Modeling and Simulation*, Pittsburgh, PA, 1995.

[37] Ryu, B. K. and Lowen, S. B. Point process approaches to the modeling and analysis of self-similar traffic: Part I - Model construction. In *Proc. IEEE INFOCOM*, San Francisco, CA, 1996.

[38] Ryu, B. K. and Meadows, H. E. Performance analysis and traffic behavior of Xphone videoconferencing application on an Ethernet. In *Proc. Third Int. Conf. Comp. Comm. Net.*, San Francisco, 1994.

[39] Saleh, B. E. A. and Teich, M. C. Multiplied-Poisson noise in pulse, particle, and photon detection. *Proc. IEEE*, 70:229–245, 1982.

[40] Taqqu, M. S. and Levy, J. B. Using renewal processes to generate long-range dependence and high variability. In E. Eberlein and M. S. Taqqu, editors, *Dependence in Probability and Statistics*, volume 11, pages 73–89. Birkhauser, Boston, MA, 1986.

[41] Teich, M. C. Fractal neuronal firing patterns. In T. McKenna, J. Davis, and S. Zornetzer, editors, *Single Neuron Computation*, pages 589–625. Academic, Boston, MA, 1992.

[42] Veitch, D. Novel models of broadband traffic. In *Proc. IEEE GLOBECOM*, Houston, TX, 1993.

[43] Willinger, W., Taqqu, M., Sherman, R., and Wilson, D. Self-similarity through high-variability: Statistical analysis of Eternet LAN traffic at the source level. In *Proc. ACM SIGCOMM*, Cambridge, MA, 1995.